Supporting Information

Cerium oxide nanoparticles inside carbon nanoreactors for selective allylic oxidation of cyclohexene

Nityananda Agasti[a]†, Maxwell A. Astle[a]*, Graham A. Rance[a,b], Jesum Alves Fernandes[a], Jairton Dupont[a,c] Andrei N. Khlobystov[a,b]*

[a] School of Chemistry, University of Nottingham, University Park, Nottingham, NG7 2RD, United Kingdom.
[b] Nanoscale and Microscale Research Centre (nmRC), University of Nottingham, University Park, Nottingham, NG7 2RD, United Kingdom.
[c] Univ Fed Rio Grande do Sul, Inst Chem, Ave Bento Goncalves 9500, BR-91501970 Porto Alegre, RS, Brazil.
*Address correspondence to Maxwell.Astle@nottingham.ac.uk; Andrei.Khlobystov@nottingham.ac.uk

S1 Thermogravimetric analysis of $Ce(tmhd)_4$

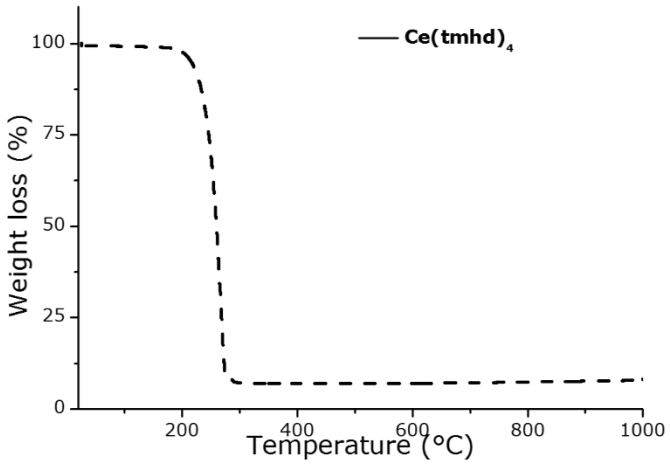

Figure S1. Thermogravimetric analysis of the $Ce(tmhd)_4$ precursor.

S2 Additional characterisation of CeO_2@GNF

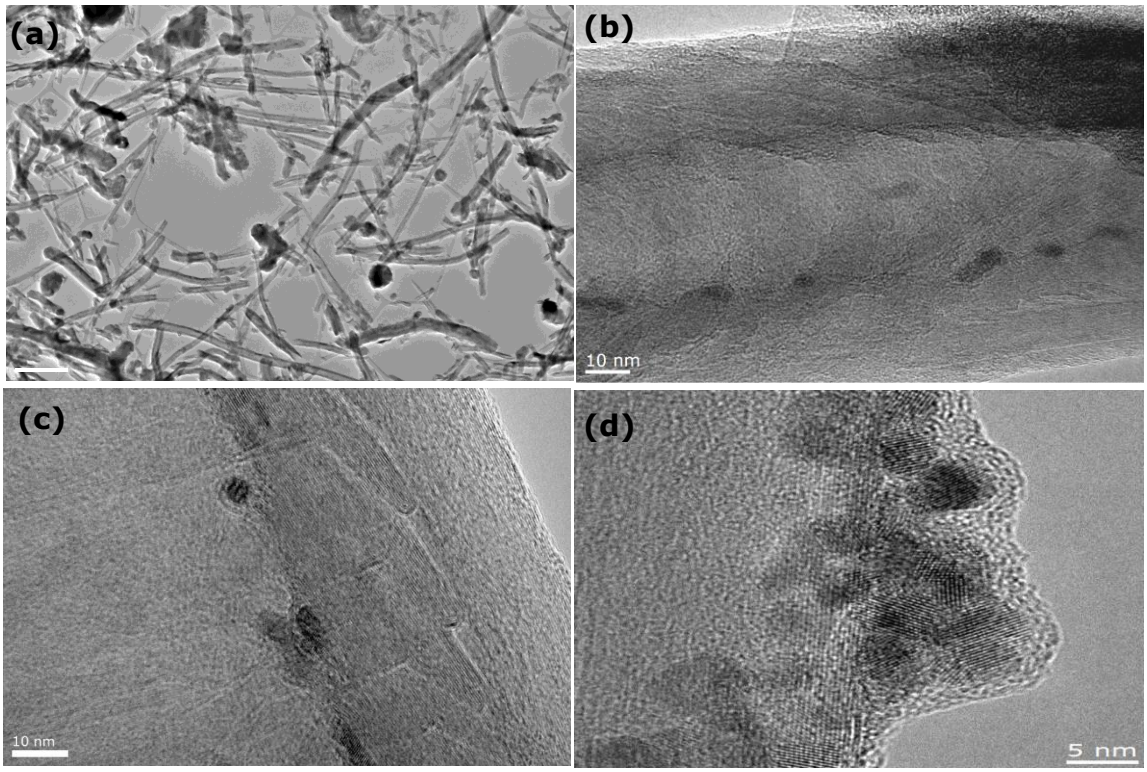

Figure S2. (a) Low and (b, c, d) high magnification HRTEM images of CeO_2@GNF-3. The low contrast, non-tubular nanostructures in (a) are damaged GNF, a consequence of the initial ball milling. The majority (> 80 %) of CeO_2 nanoparticles reside at the graphitic step-edges inside GNF (b, c), with only a small number of clustered nanoparticles observed on the GNF outer surface of GNF (d).

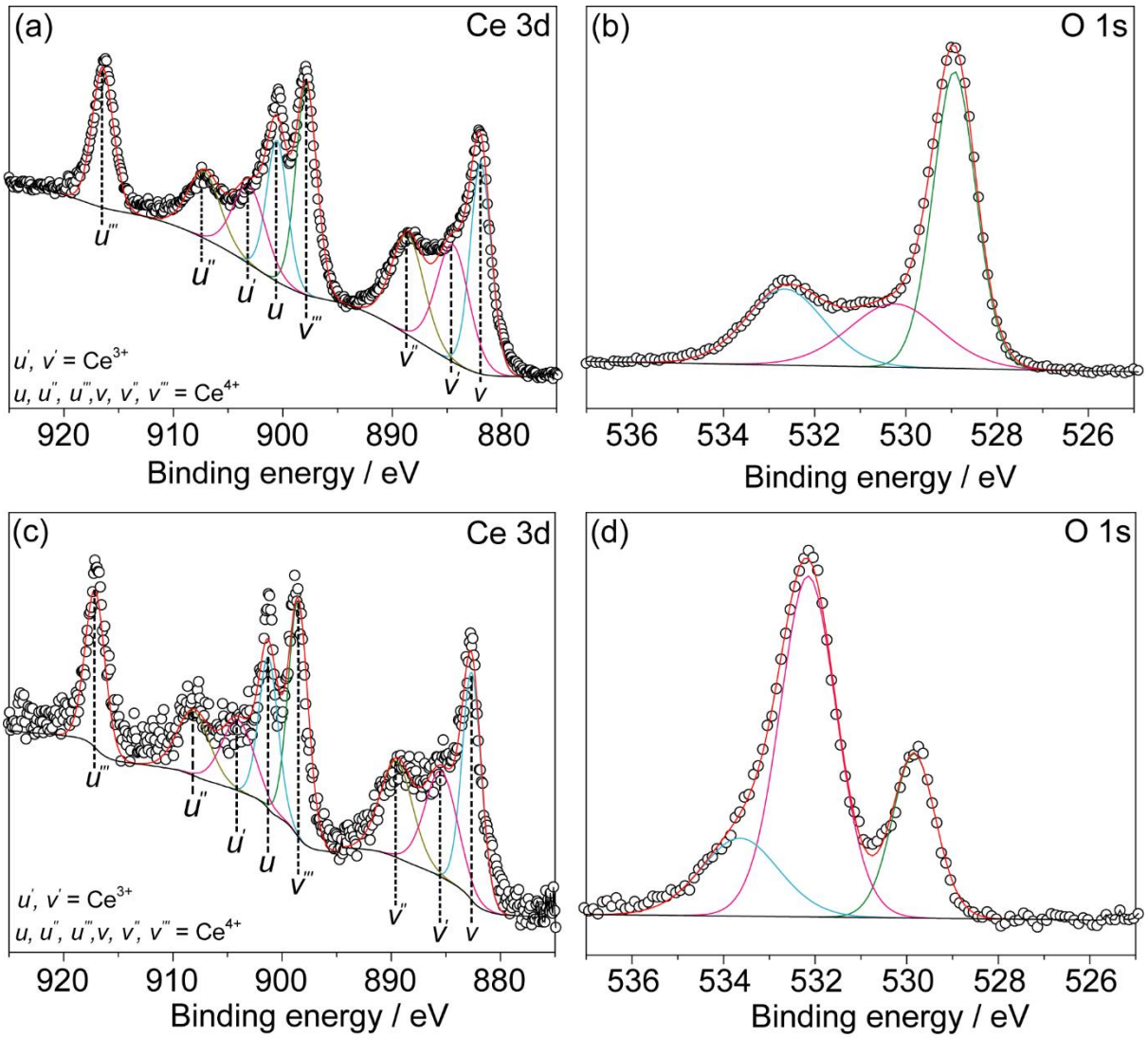

Figure S3. XPS analysis of CeO_2@GNF before (a, b) and after the cyclohexene oxidation reaction (c, d).

Table S1. XPS fitting of the Ce 3d signal. Integrated peak areas expressed as percentage of the total fit are included in parentheses.

	V / eV	V′/ eV	V″/ eV	V‴/ eV	u / eV	u′ / eV	u″ / eV	u‴ / eV
Ce 3d	881.9 (18.0%)	884.2 (12.8%)	888.4 (11.2%)	897.8 (18.3%)	900.5 (11.9%)	902.8 (8.4%)	907.0 (7.4%)	916.4 (12.0%)
C 3d (after reaction)	882.6 (17.0%)	885.4 (13.1%)	889.5 (12.1)	898.5 (18.0%)	901.2 (11.2%)	904.0 (8.8%)	908.1 (8.0%)	917.12 (11.8%)

Table S2. XPS fitting of the O 1s signal. Integrated peak areas expressed as percentage of the total fit are included in parentheses.

	lattice oxygen (O^{2-}) / eV	Oxygen vacancies/hydroxyl groups / eV	water / eV
O 1s	529.0 (52.05)	530.3 (23.70)	532.7 (24.25)
O 1s (after reaction)	529.8 (22.0%)	532.2 (59.3%)	533.6 (18.6%)

The Ce 3d core peaks were deconvoluted into eight components associated with Ce^{4+} (78.8 at%) and Ce^{3+} (21.2 at%).[S1-S3] The O 1s was fit with three components: a main peak at 529.3 eV attributed to lattice oxygen, i.e. oxygen bound to Ce^{3+} and Ce^{4+}; a second peak at 531.1 eV associated with the presence of hydroxide and oxygen vacancies in the structure and a third peak located at higher binding energy (533.15 eV) ascribed to adsorbed water molecules and organic compounds.[S3,S4]

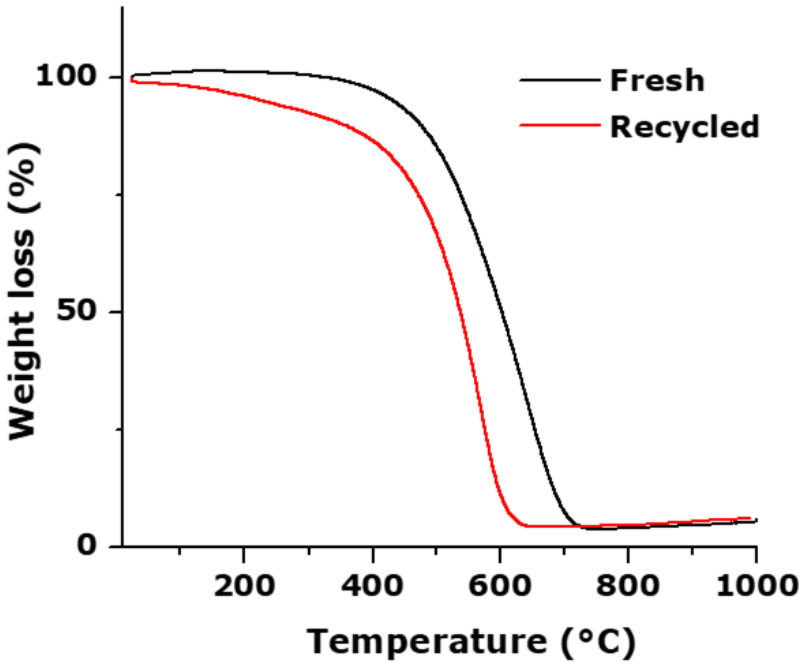

Figure S4. Thermogravimetric analysis of fresh CeO_2@GNF and after five uses in the oxidation of cyclohexene.

S3 Oxidation of cyclohexene

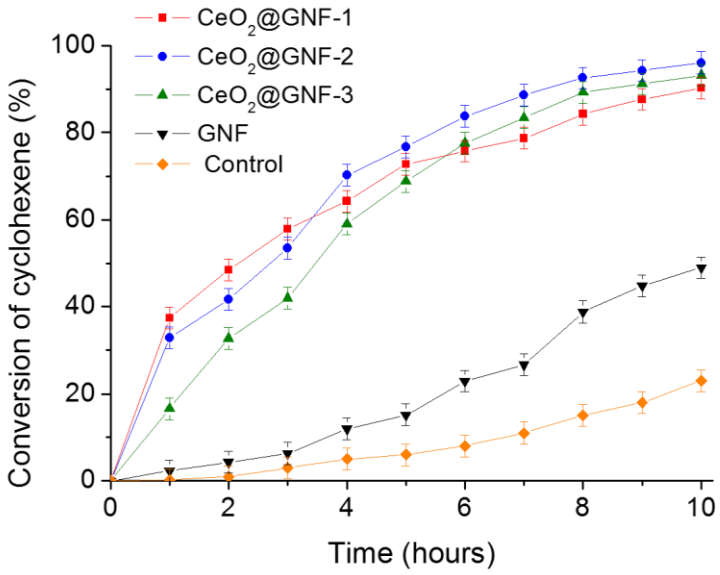

Figure S5. The conversion of cyclohexene using CeO_2@GNF.

Table S3. The effects of CeO_2 loading, particle size and nature of carbon support on the conversion of cyclohexene and distribution of the afforded products.

Species [a]	CeO_2 loading (mol %) [b]	Particle size (nm) [c]	Conversion (%) [d]	Selectivity (%) (1):(2):(3):(4)(5) [d]
None	-	-	18	50:0:0:50:0
GNF	-	-	44	60:22:18:0:0
graphite	-	-	14	98:2:0:0:0
activated carbon	-	-	45	78:15:7:0:0
CeO_2@GNF-1	0.11	4.6±0.2	87	75:25:0:0:0
CeO_2@GNF-2	0.13	6.2±0.6	94	66:34:0:0:0
CeO_2@GNF-3	0.17	8.5±0.3	91	63:37:0:0:0

[a] Reaction conditions: cyclohexene (2.9 mmol), TBHP oxidant (5.8 mmol), CeO_2@GNF (0.004 mmol), 1,4-dichlorobenzene internal standard (1.44 mmol), acetonitrile (2.5 mL), 9 hours, 80 ^oC . [b] Determined by TGA. [c] Determined by TEM. [d] Determined by ^1H NMR spectroscopy.

Whilst comparison of CeO_2@GNF with different mass loadings of CeO_2 did not reveal significant differences in terms of cyclohexene conversion, a slightly higher conversion was observed for CeO_2@GNF-2, where the average nanoparticle size is ~6 nm (cf. ~4 and 9 nm for CeO_2@GNF-1 and CeO_2@GNF-3, respectively). The lower cyclohexene conversion obtained with CeO_2@GNF-1 with CeO_2 particle size ~4 nm could be attributed to the higher nanoparticle surface energy leading to strong binding of reaction intermediates which subsequently hinders their dissociation to form products, i.e. a poisoning effect.[S5,S6] With the highest mass loading of CeO_2, comparatively fewer CeO_2 particles are confined inside GNF,

leading to lower conversion with CeO_2@GNF-3. A similar non-linear ('volcano'-like) variation in the activity with particle size was reported for Au nanoparticles catalysing the decomposition of H_2O_2.[S7]

Table S4. Comparison of this work with previous literature reports on the oxidation of cyclohexene through allylic and olefinic oxidation, yielding 2-cyclohexenyl hydroperoxide (**1**), 2-cyclohexenone (**2**), 2-cyclohexenol (**3**), cyclohexane epoxide (**4**) and 1,2-cyclohexanediol (**5**).

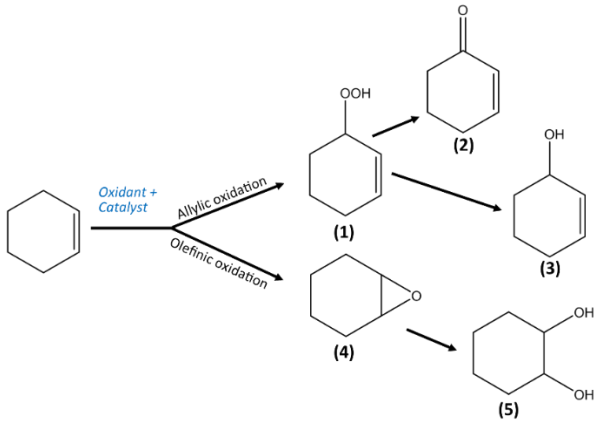

Species	CeO_2 loading (mol%)	Conversion (%)	Selectivity (%)					Ref.
			(1)	(2)	(3)	(4)	(5)	
CeO_2@GNF [a]	0.13	94	66	34	0	0	0	This work
VO_2/CeO_2 [b]	2.00	45	0	18	5	77	0	53
CeO_2 nanorods [c]	11.60	22	86	<14	<14	0	0	S8
CeO_2 [d]	5.22	76	0	67	33	0	0	S9
Mn/CeO_2 [e]	17.40	52	-	52	26	-	-	S10

[a] Reaction conditions: cyclohexene (2.9 mmol), TBHP oxidant (5.8 mmol), CeO_2@GNF (0.004 mmol), 1,4-dichlorobenzene (1.44 mmol) (internal standard), acetonitrile (2.5 mL), 9 hours, 80 °C. [b] Reaction conditions: cyclohexene (29.0 mmol), TBHP (38.45 mmol), VO_2/CeO_2 (0.581 mmol), *n*-heptane (25 mL), 6 hours, 65 °C. [c] Reaction conditions: cyclohexene (1.5 mmol), TBHP oxidant (3.0 mmol), CeO_2 nanorods (0.174 mmol), acetonitrile (1.5 mL), 24 hours, 55-105 °C, specific selectivity for (**2**) and (**3**) not discussed. [d] Reaction conditions: cyclohexene (10 mmol), H_2O_2 (213.1 mmol), CeO_2 (0.522 mmol), 24 hours, 82-85 °C. [e] Reaction conditions: cyclohexene (1 mmol), O_2 (10 bar), Mn/CeO_2 (0.174 mmol), anisole (1mmol) (internal standard), acetonitrile (5 mL), 4 hours, 110 °C, selectivity of all the products not discussed.

S4 Characterisation of CeO_2@graphite

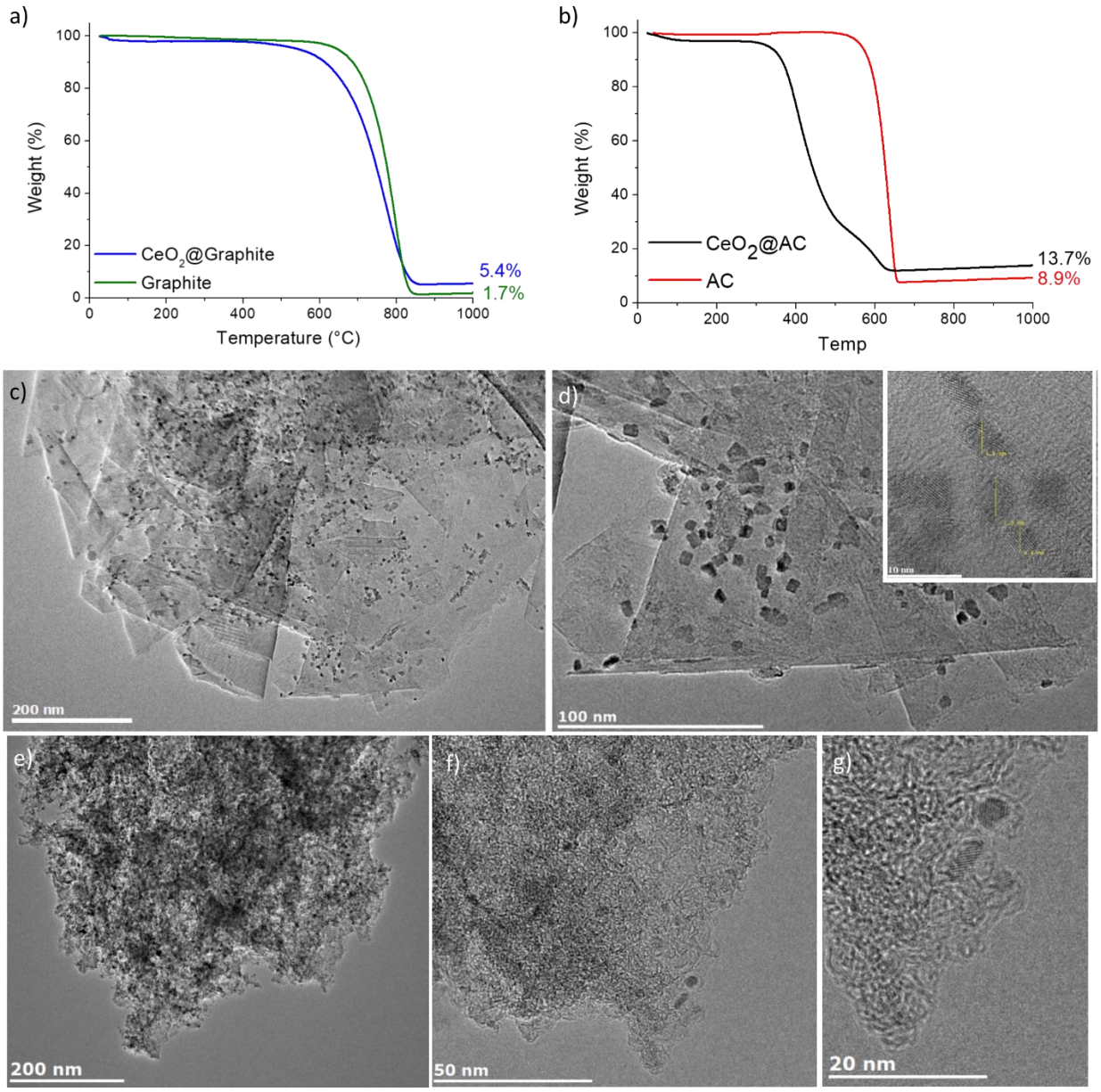

Figure S6. TGA of CeO_2@graphite vs graphite (a) and CeO_2@AC vs AC (b). The small shift in combustion temperature after deposition of CeO_2 on graphite noted in (a) indicates low intimacy of contact between CeO_2 and graphite; a larger shift in the combustion temperature subsequent to formation of CeO_2 on AC in (b) confirms the catalytic effect of CeO_2 on the oxidation of AC in air, similar to that seen for CeO_2@GNF. TEM images of CeO_2@graphite (c,d) and CeO_2@AC (e,f,g) show the homogeneous loading of CeO_2 on both carbon supports: on graphite as pseudo-cubic nanoparticles, whereas on AC pseudospherical nanoparticles are noted.

S5 References

[S1] Arndt, B.; Noei, H.; Keller, T.F.; Muller, P.; Vonk, V.; Nenning, A.; Opitz, A.K.; Fleig, J.; Rutt, U.; Stierle, A. Structure and stability of Gd-doped CeO_2 thin films on yttria-stabilized zirconia, *Thin Solid Films*, **2016**, *603*, 56-61.

[S2] Wang, N,; Qian, W.; Chu, W.; Wei. F. Crystal-plane effect of nanoscale CeO_2 on the catalytic performance of Ni/CeO_2 catalysts for methane dry reforming, *Cat. Sci. Technol.*, **2016**, *6*, 3594-3605.

[S3] Pereira, A.; Blouin, M.; Pillonnet, A.; Guay, D. Structure and valence properties of ceria films synthesized by laser ablation under reducing atmosphere, *Mater. Res. Express*, **2014**, *1*, 015704.

[S4] Dupin, J.-C.; Gonbeau, D.; Vinatier, P.; Levasseur, A. Systematic XPS studies of metal oxides, hydroxides and peroxides, *Phys. Chem. Chem. Phys.*, **2000**, *2*, 1319-1324.

[S5] Samai, B.; Sarkar, S.; Chall, S.; Rakshita, S.; Bhattacharya, S.C. Polymer-fabricated synthesis of cerium oxide nanoparticles and applications as a green catalyst towards multicomponent transformation with size-dependent activity studies, *CrystEngComm*, **2016**, *18*, 7873-7882.

[S6] Guo, K.; Li, H.; Yu, Z. Size-dependent catalytic activity of monodispersed nickel nanoparticles for the hydrolytic dehydrogenation of ammonia borane, *ACS Appl. Mater. Interfaces*, **2018**, *10*, 517-525.

[S7] Kiyonaga,T.; Jin, Q.; Kobayashi, H.; Tada, H. Size-dependence of catalytic activity of gold nanoparticles loaded on titanium (IV) dioxide for hydrogen peroxide decomposition. *ChemPhysChem*, **2009**, *10*, 2935-2938.

[S8] Macedo, A. G.; Fernandes, S. E. M.; Valente, A. A.; Ferreira, R. A. S.; Carlos, L. D.; Rocha, J. Catalytic performance of ceria nanorods in liquid-phase oxidations of hydrocarbons with tert-butyl hydroperoxide. *Molecules*, **2010**, *15*, 747-765

[S9] Sutradhar, N.; Sinhamahapatra, A.; Pahari, S.; Jayachandran, M.; Subamanian, S.; Bajaj, H.C.; Panda, A.B. Facile Low-Temperature Synthesis of Ceria and Samarium-Doped Ceria Nanoparticles and Catalytic Allylic Oxidation of Cyclohexene, *J.Phys. Chem. C*, **2011**, 115, 7628-7637.

[S10] Zhang, P.; Lu, H.; Zhou, Y.; Zhang, L.; Wu, Z.; Yang, S.; Shi, H.; Zhu, Q.; Chen, Y.; Dai, S. Mesoporous MnCeOx solid solutions for low temperature and selective oxidation of hydrocarbons, Nat. Commun., 2015, 6, 8446, 1-10.